RSC Advances

PAPER

View Article Online
View Journal | View Issue

Cite this: *RSC Adv.*, 2024, **14**, 36602

Selectively electrolyzing CO_2 to ethylene by a Cu–Cu_2O/rGO catalyst derived from copper hydroxide nanostrands/graphene oxide nanosheets†

Chenxiang Peng,[a] Bing Yao,[bc] Lei Wang[b] and Xinyi Wan *[bc]

Received 9th October 2024
Accepted 30th October 2024

DOI: 10.1039/d4ra07259f

rsc.li/rsc-advances

Electrolyzing CO_2 into ethylene (C_2H_4) is a promising strategy for CO_2 utilization and carbon neutrality since C_2H_4 is an important industrial feedstock. However, selectively converting CO_2 into C_2H_4 *via* the CO_2 electro-reduction reaction (CO_2 ERR) is still a great challenge. Herein, Cu–Cu_2O nanoparticles anchored on reduced graphene oxide nanosheets (Cu–Cu_2O/rGO) were prepared from copper hydroxide nanostrands (CHNs) and graphene oxide (GO) nanosheets *via in situ* electrochemical reduction. Cu–Cu_2O nanoparticles with diameter less than 10 nm were formed on the surface of rGO nanosheets. After assembling the Cu–Cu_2O/rGO catalyst into a flow cell, it demonstrated high Faraday efficiencies (FEs) of 55.4%, 37.6%, and 6.7% for C_2H_4, C_2H_6, and H_2, respectively, and a total 93% FE for C_2 at −1.3 V *vs.* the standard hydrogen electrode (SHE). Moreover, its FE was 68.2% for C_2H_4, 10.2% for C_2H_6, and 20.5% for H_2 at −1.4 (*vs.* SHE). Besides, no liquid carbon product was detected. This high selectivity is attributed to the synergistic effect arising from the small diameter of Cu–Cu_2O NPs with the combination of Cu^0–Cu^+ and rGO nanosheets, which promotes the activation of CO_2 molecules, facilitates C–C coupling, and enhances stability. This may provide a facile way for designing an efficient catalyst for selectively electrolyzing CO_2 into valuable C_2 chemicals.

Introduction

CO_2 electro-reduction into valuable chemicals is a desirable way for carbon neutralization.[1] Tremendous attention has been paid to design novel catalysts to produce ethylene (C_2H_4), an important chemical feedstock, from CO_2 *via* the CO_2 electro-reduction reaction (ERR).[2–4] Among them, the most promising are Cu-based catalysts owing to their unique electronic structures, which exhibit high CO_2 activation ability and moderate CO adsorption affinity and facilitate the formation of C_2H_4.[5–7] It has been found that copper crystal facets,[8] copper oxidation states,[9] crystal size,[10] interaction between nanocrystals,[11] grain boundaries,[12] coordination environments,[13] electrolytes[14] and so forth could significantly affect the performance for electrolyzing CO_2 to C_2H_4. Some researchers have confirmed that the Cu^+ state in the Cu/Cu_2O catalyst plays a critical role in the selective formation of C_2H_4.[3,5,9–12] For example, Zhang *et al.* prepared Cu/Cu_2O convex spheres with an adjustable Cu^0–Cu^+ interface to improve C_2 production by modulating hydrothermal synthesis time.[11] Gong's group also found that the synergism of Cu^0–Cu^+ pairs could enhance CO_2 ERR activity. Cu^0 activates CO_2 and facilitates electron transfer, while Cu^+ forces *CO adsorption and boosts C–C coupling.[12] Most Cu^0–Cu^+ catalysts were prepared *via* the hydrothermal process from copper salts with a reducing agent.[11,12] The hydrothermal process may be energy intensive like a black box and not easily controllable. In addition, the preservation of the oxidation of Cu^+ in the Cu^0–Cu^+ catalyst during the CO_2 EER process is still a challenge.[13–17] Recently, it has been proposed that carbon-based materials,[13–17] including C_{60},[14,15] graphene-related materials[16] and carbon nanotubes (CNTs),[17] could enhance the stability of the Cu^+ state of Cu–Cu^+ during the CO_2 EER process. Meanwhile, it is well known that the smaller the catalyst size, the higher the activity.[2–5]

In this work, we prepared Cu^0–Cu^+ (Cu–Cu_2O) nanoparticles with a diameter less than 10 nm anchored on reduced graphene oxide (rGO) nanosheets, named as Cu–Cu_2O/rGO, *via in situ* electrochemical reduction from a composite composed of 2 nm copper hydroxide nanostrands/graphene oxide nanosheets (CHNs/GO). It has been reported that the CHNs are highly positively charged.[18] In addition, it is well known that GO nanosheets are negatively charged.[19] Therefore, due to the strong electrostatic interaction, the CHNs and GO were well assembled together to form the CHNs/GO composite, similar to those reported.[19] After drop-casting CHNs/GO with Nafion on

[a]*Department of Chemistry, Zhejiang University, Hangzhou 310058, P. R. China*
[b]*State Key Laboratory of Silicon and Advanced Semiconductor Materials, School of Materials Science and Engineering, Zhejiang University, P. R. China. E-mail: 11826060@zju.edu.cn*
[c]*Wenzhou Key Laboratory of Novel Optoelectronic and Nanomaterials, Institute of Wenzhou, Zhejiang University, Wenzhou 325006, P. R. China*

† Electronic supplementary information (ESI) available. See DOI: https://doi.org/10.1039/d4ra07259f

a gas diffusion electrode, it was *in situ* electrochemical reduced to Cu–Cu_2O/rGO in a flow cell. It demonstrated high selectivity and stable performance for CO_2 ERR. The Faraday efficiency (FE) of C_2H_4 was 55.4% and 68.2% at −1.3 V and −1.4 V *vs.* standard hydrogen electrode (SHE), respectively, while it is 37.6% and 10.2% for C_2H_6. No liquid product was detected. This holds potential for the synthesis of efficient Cu-based catalysts for the electrolysis of CO_2 to C_2H_4.

Experimental

Chemicals and materials

Copper nitrate ($Cu(NO_3)_2 \cdot 3H_2O$), 2-aminoethanol (NH_2–CH_2-CH_2OH, AE), and potassium bicarbonate ($KHCO_3$) were purchased from ACROS Chemicals. Ethanol and isopropanol were purchased from Sinopharm Chemical Reagent Co. Ltd. Graphene oxide nanosheets dispersion with diameter of about 1 micrometer was purchased from GaoxiTech Co. Ltd. Nafion was purchased from Sigma-Aldrich. Ultrapure water with 18.2 MΩ cm, resistivity produced by a Millipore direct-Q system (Millipore), was used throughout the experiments. All materials used in this work were used without further purification.

Synthesis of CHNs

The CHNs were prepared by mixing equal volume of 4 mM $Cu(NO_3)_2$ and 1.6 mM AE aqueous solution under stirring for 5 min, then aged for 2 days at room temperature, as described elsewhere.[18]

Synthesis of the CHNs/GO composite

The CHNs/GO composite was typically synthesized by mixing 2 mL 2 mg mL^{-1} GO aqueous solution (zeta potential − 46 mV) with a certain volume of CHNs solution under stirring for 10 min following the process reported elsewhere.[19] Then, the gel-like precipitate was collected by centrifugation at 8000 rpm and dried at room temperature overnight. CHNs/GO with various volume ratios of CHNs to GO were prepared, as listed in Table S1.†

Synthesis of the Cu–Cu_2O/rGO composite

The dried CHNs/GO 10 mg powders, 0.02 mL Nafion solution, 0.96 mL isopropanol, and 1 mL water were mixed together and ground for 30 min. Then, this mixture was cast on the gas diffusion electrode (or porous carbon paper) with a loading amount of 2 mg cm^{-2} and dried under infrared light (0.1 W cm^{-2}) for 3 hours. After drying, the electrode loaded with CHNs/GO was electrochemically reduced to Cu–Cu_2O/rGO in 0.5 M $KHCO_3$ solution, with CO_2 flow rate of 20 mL min^{-1}, under −3 V *vs.* SHE for 1 hour in the flow cell. The counter electrode was a Pt foil. The reference electrode was the Ag/AgCl electrode.

Characterization

The crystalline data were collected on an X-ray powder diffractometer (SmartLab, 5°–70°, Cu K_α). Scanning electron microscopy (SEM, Ultra 55) with X-ray energy-dispersive spectroscopy (EDS) and transmission electron microscopy (TEM, HT7700) were used. The X-ray photoluminescence spectra (XPS) were recorded employing an XPS AXIS SUPRA (Kratos, UK). Liquid-phase products were detected by ^1H nuclear magnetic resonance (NMR) spectroscopy (Bruker AVANCE AV III 500 MHz). 400 μL catholyte was added in 50 μL dimethyl sulfoxide (DMSO) (6 mM) solution as the internal standard and 50 μL D_2O as the identification and quantification of liquid products. The spectra were measured with water suppression by excitation sculpting. Online gas chromatography (GC, FuLi 9790II) equipped with a flame ionization detector (FID) and a thermal conductivity detector (TCD) was employed to quantify the gas products.

CO_2 ERR test

The CO_2 ERR test was carried out in home-made flow cell assembled with an anion exchange membrane on an electrochemical workstation CHI 760E, with Pt foil counter electrode, Ag/AgCl reference electrode, and the gas diffusion electrode loaded with the catalyst working electrode. The electrolyte was 1 M $KHCO_3$ aqueous solution (pH 8.4) for CO_2 ERR, while it was 0.5 M $KHCO_3$ aqueous solution (pH 8.2) for CHNs/GO reduction and activation. CO_2 gas (99.99%) with 20 mL min^{-1} flow rate was filled. The effective area of the working electrode was 1 cm^2.

Linear sweep voltammetry (LSV) was recorded by a flow cell with 20 mL min^{-1} flow rate of CO_2 and 1 M KOH. The electrolyte (1 M KOH) was circulated at a flow rate of 10 mL min^{-1} by a pump. The potential was converted to the SHE without internal resistance correction.

In situ FTIR and Raman measurement

The *in situ* attenuated total reflection-surface enhanced infrared absorption spectroscopy (ATR-SEIRS) were recorded by an infrared spectrometer (Nicolet 6700) equipped with a liquid nitrogen cooled mercury–cadmium–telluride (MCT-A) detector. A homemade cell was assembled on top of the Si prism. First, an Au layer was chemically deposited on the Si prism. Then, the catalysts were loaded on the Au-coated Si prism and used as the working electrode. A Pt wire and Ag/AgCl served as the counter electrode and reference electrode, respectively. 0.1 M KOH was used as the electrolyte. After running for 100 s, the FTIR spectra were collected with a resolution of 8 cm^{-1} in the range from 1000 to 4000 cm^{-1} under a certain potential. In order to monitor the CHNs of the CNHs/GO conversion in the Cu–Cu_2O process, *in situ* Raman spectra were recorded by a LabRAM Odyssey™ (HORIBA France SAS) using the same homemade cell with 0.5 M $KHCO_3$ solution and CO_2 flow rate of 20 mL min^{-1} at −3 V *vs.* SHE.

Results and discussion

Fabrication and characterization of Cu–Cu_2O/rGO

The typical synthesis process of Cu–Cu_2O/rGO is illustrated in Scheme 1. The highly positively charged CHNs were prepared by adding AE solution into $Cu(NO_3)_2$ under stirring following the method described by Prof. Ichinose.[18] They confirmed that half of the surface copper atoms of the CHNs are positively charged

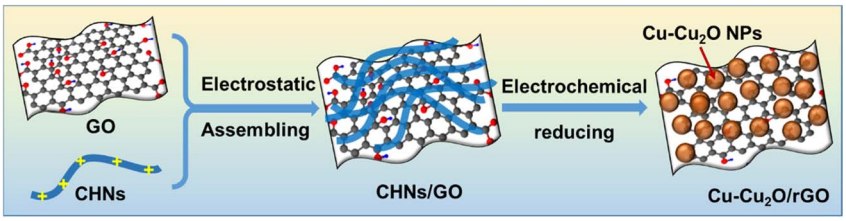

Scheme 1 Illustration of the synthesis process of Cu–Cu_2O/rGO from CHNs/GO *via in situ* electrochemical deposition.

by adsorbing negatively charged dyes. The SEM image (Fig. S1a†) and TEM image (Fig. 1d) indicate that the linear structure of CHNs with diameter of about 2 nm is successfully formed, as reported elsewhere.[18] The CHNs/GO composites were formed by mixing CHNs with GO solution *via* electrostatic interaction as described by Prof. Peng for molecular separation membrane.[19] The microstructures of the CHNs/GO prepared from 125 mL CHNs and 1 mL GO solution (2 mg mL^{-1}) are presented in Fig. 1a and e. Due to the highly charged surface of CHNs[18] and negatively charged surface of the GO nanosheet, it is obvious that the ultrafine fibrous CHNs and GO nanosheets are uniformly assembled together *via* electrostatic interaction. Similar morphology was observed for the CHNs/GO with a volume ratio of CHNs to GO of 100 : 1 and 150 : 1 (Fig. S1b and c†), respectively. The CHNs/GO was further mixed with Nafion and drop casted on a gas diffusion electrode (or porous carbon paper). An electrochemical reduction was applied to convert CHNs/GO to Cu–Cu_2O/rGO in 0.5 M $KHCO_3$ electrolyte under −3 V *vs.* SHE for 1 hour. The samples prepared from various volume ratios of CHNs solution and GO solution (2 mg mL^{-1}) were named as S1 to S11 (see details in Table S1†). The SEM images of the S10 Cu–Cu_2O/rGO catalyst (prepared from 125 CHNs and 1 mL 2 mg mL^{-1} GO) are shown in Fig. 1b (high magnification), Fig. 1c and S2† (large scale view), respectively. After electrochemical reduction, the fibrous CHNs disappeared, while nanoparticles with uniform size of less 10 nm were formed and anchored on the surface of the wrinkled rGO sheets. The wrinkled surface with grooves is rough and resulted in a high active surface area for the electrochemical reaction. The TEM image (Fig. 1f) of the Cu–Cu_2O/rGO (S10) further confirms that the size of the nanoparticles is several nanometers. The corresponding SEM EDS element mapping images (Fig. 2) indicate Cu, C, and O are uniformly distributed in the sample. It also shows the overlapping part of Cu and O (Fig. 2b and c). All of these mean that the particles are mostly Cu and Cu–O species.

The XRD patterns of the S10 Cu–Cu_2O/rGO sample before and after electrochemical reduction are shown in Fig. 3a. Two strong peaks at 43.3° and 50.4° are indexed to the (111) and (200) planes of Cu, respectively (JCPDS 04-0836).[7,11] The small peak located at 36.4° is assigned to the (111) plane of Cu_2O (JCPDS 005-0667).[7,11] No peaks for crystalline CuO were observed. The broad peak at 25° is indexed to rGO.[20] These results indicate that the major products of the electrochemical reduction of CHNs are Cu with minor Cu_2O. Similar results for S9 and S11 were achieved, as shown in Fig. S3.† In order to

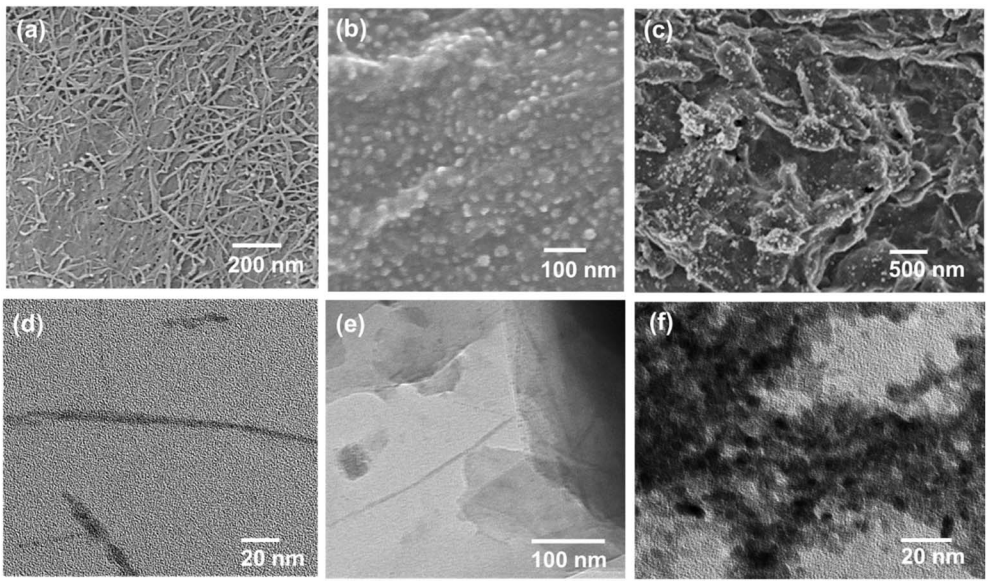

Fig. 1 (a) SEM image of CHNs/GO prepared from 125 mL CHNs and 1 mL 2 mg mL^{-1} GO. (b and c) SEM images of the sample S10 Cu–Cu_2O/rGO after *in situ* electrochemical reduction. (d) The TEM image of CHNs. (e) TEM image of CHNs/GO. (f) TEM image of Cu–Cu_2O/rGO.

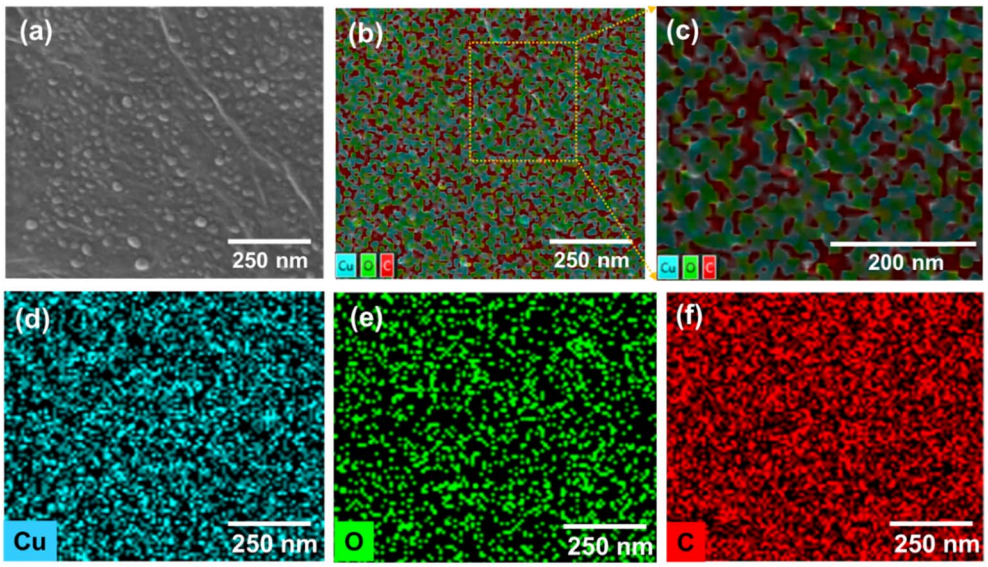

Fig. 2 (a) SEM image of S10 Cu–Cu_2O/rGO with EDS mapping. The corresponding EDS mapping images; (b) overall elements combined together; (c) enlarged section of (b); (d) Cu, (e) oxygen and (f) carbon.

monitor the CHNs electrochemical reduction process, the *in situ* Raman spectra (Fig. S4†) in the range from 200 to 700 cm^{-1} were recorded during the electrochemical reduction of CHNs/GO. The characteristic peaks at about 292 and 470 cm^{-1} assigned to $Cu(OH)_2$ (ref. 21 and 22) continuously decline and finally disappear after 1 hour, while the peak at about 525 cm^{-1} indexed to Cu_2O[21,22] is clearly observed after 15 min and up to 1 hour. These results indicate the Cu_2O phase is really formed during the electrochemical reduction. The formation of Cu–Cu_2O is further supported by the XPS results (Fig. 3d and 4) recorded for S10 before and after electrochemical reduction. Fig. 3d is the corresponding survey scan XPS spectra. It clearly demonstrates the Cu 2p, O 1s and C 1s peaks.[7,9,11] The atomic percent of these elements are 11.09 at% for Cu, 35.26 at% for O, and 53.65 at% for C in CHNs/GO. After electrochemical reduction, Cu is almost the same while oxygen significantly deceases to 17.17 at% and C dramatically increases to 72.66 at% (inset table in Fig. 3b). These mean that the reduction of CHNs and GO occurs. Fig. 4a, b and d–f are the corresponding high resolution Cu 2p, O 1s and C 1s XPS spectra of CHNs/GO and Cu–Cu_2O/rGO, respectively.

It is clearly seen that before electrochemical reduction, the Cu valent state is Cu^{2+} with typical XPS spectrum having two obvious satellite peaks at 942 and 945 eV (Fig. 4a) in CHNs/GO, while, it is Cu^0 and Cu^+ with overlapped two strong peaks and small satellite peaks after reduction in Cu–Cu_2O/rGO (Fig. 4b).[9,11,23–30] To more clearly distinguish the valent sate of Cu^0 and Cu^+, the Cu LMM spectra (Fig. 4c) were recorded. The

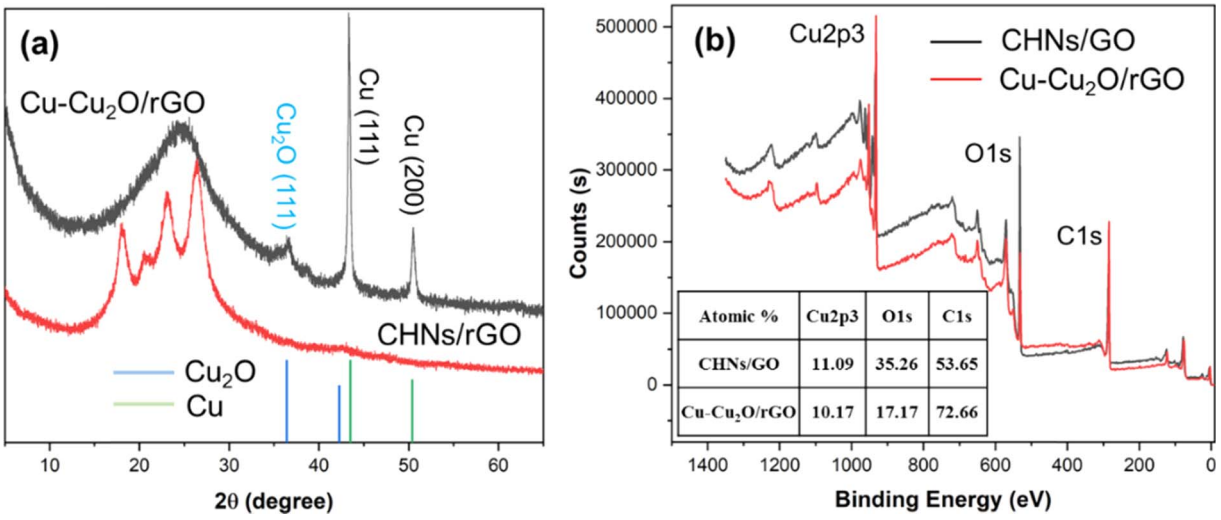

Fig. 3 (a) The XRD patterns and (b) survey scan XPS spectra of S10 before (CHNs/GO) and after electro-reduction (Cu–Cu_2O/rGO). The inset table in (b) lists the atomic ratio of Cu, O, and C of S10 before and after electro-reduction, calculated from the XPS results.

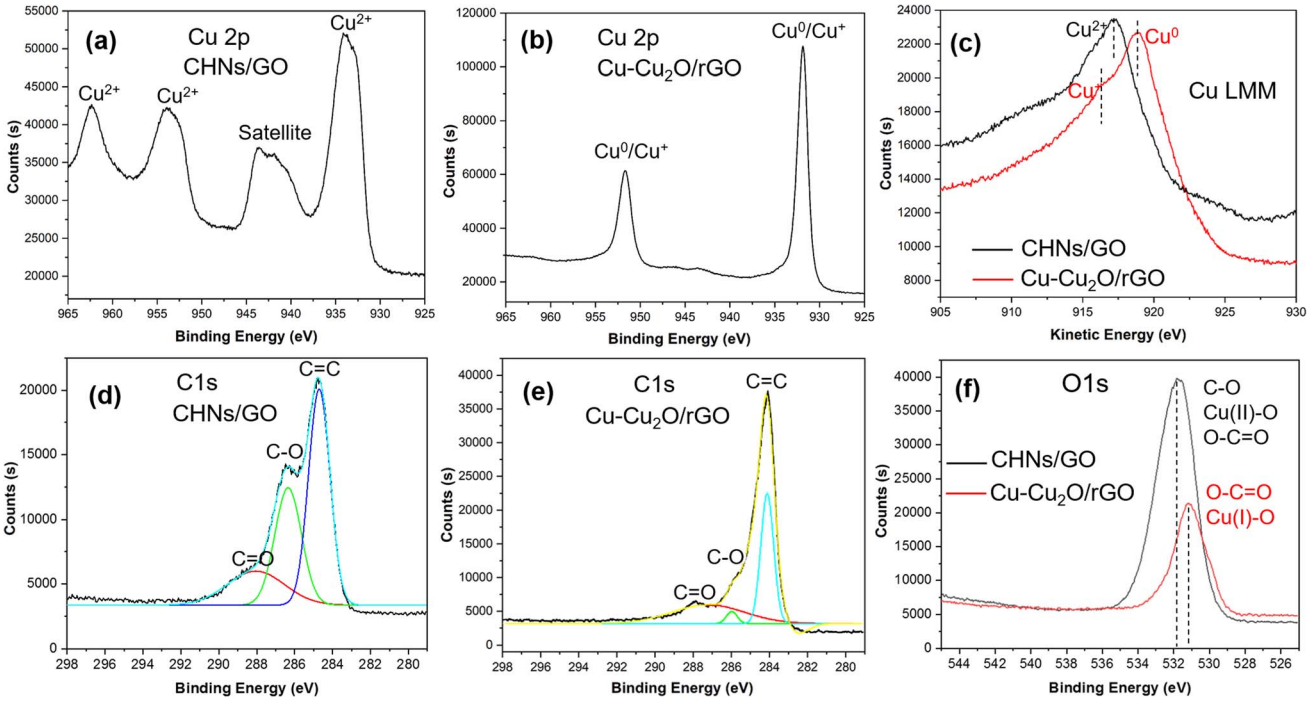

Fig. 4 High resolution XPS spectra of (a and b) Cu 2p, (c) Cu LMM, (d and e) C 1s; (f) O 1s of S10 before (CHNS/GO) and after (Cu–Cu_2O/rGO) electro-reduction.

typical XPS LMM Cu^{2+} peak of CHNs/GO is observed, while a strong Cu^0 peak with a weak shoulder Cu^+ peak in the XPS LMM spectrum of Cu–Cu_2O/rGO is seen.[9,11,24,27] Comparing the C 1s spectra of CHNs/GO (Fig. 4d) with that of Cu–Cu_2O/rGO (Fig. 4e), the C–O, C=O peaks significantly decrease. Similar decrease trends of C–O and Cu(II)=O peaks are also observed in the O 1s spectra (Fig. 4f).[31,32] The intensity of O 1s from the Cu^{2+}=O and C–O peaks dramatically declines.[9,11,32,33] In addition, the total intensity of O 1s is significantly decreased after reduction. These mean that both CHNs and GO are really reduced. Based on the weak Cu_2O peak in the XRD pattern (Fig. 3a) and small shoulder peak of Cu^+ in the Cu LMM spectrum (Fig. 4f), the atomic ratio of Cu^+ to Cu in the Cu–Cu_2O/rGO (S10) calculated by Gauss-fitting is about 10%.

CO_2 ERR performance

The aforementioned XRD, *in situ* Raman and XPS results confirmed the formation of the Cu–Cu_2O/rGO composite. It has been reported that the Cu^0–Cu^+ combination is desirable for selectively converting CO_2 to C_2H_4 by the CO_2 ERR process.[3,5,7,9,11,12,14,17] It has also been confirmed that carbon-based supports for copper-based catalyst could enhance their stability during the CO_2 ERR process.[7,13–17] Therefore, the prepared Cu–Cu_2O/rGO samples were examined for CO_2 ERR. Linear sweep voltammetry (LSV) investigation was carried out using a flow cell under CO_2 flow in 0.5 M $KHCO_3$ electrolyte to study the activity of the resulting samples. A typical activation curve of S10 is shown in Fig. S5a.† It is clearly seen that the catalyst shows onset activity at −1.1 V *vs.* SHE. The chronoamperometry curves of S10 at different potentials is shown in Fig. S5b.† The current increases from −1.3 to −1.8 V *vs.* SHE. It is critical to suppress H_2 evolution during the CO_2 ERR.[30–34] In order to find the appropriate sample with less H_2 evolution, the FE of H_2 by the catalysts prepared from different volume ratios of CHNs to GO, from S1 to S11, under −1.3 V *vs.* SHE were calculated from the gas products during the operation (Fig. S6†). Fig. S6† indicates that the FE of H_2 increases from 8.2% to about 12% with the volume ratio of CHNs to GO in the range from 5 : 1 up to 20 : 1. Then, it declines to about 6.7% for the volume ratio of CHNs to GO at 125 : 1 (S10) and slightly increases when the volume ratio is 150 : 1 (S11). The FE calculation follows the methods described elsewhere.[2–17,21–30,33–37] It is clear that S10 is the optimal catalyst, which has the lowest FE of H_2. Therefore, S10 was chosen to investigate the CO_2 ERR performance in detail. Fig. S5b† is the chronoamperometric curves of S10 under various potentials. The NMR results (Fig. S7–S12†) indicate that there are no liquid carbon products in the potential range from −1.3 to −1.8 V *vs.* SHE. The corresponding FE of the gas products are shown in Fig. 5a and Table S2.† The FE of C_2H_4, C_2H_6, H_2 and CO are 55.4%, 37.6%, 6.7% and 0.3%, respectively, at −1.3 V *vs.* SHE. The total FE for C_2H_4 and C_2H_6 is 93%. When the potential is −1.4 V *vs.* SHE, the FE of C_2H_4, C_2H_6, H_2 and CO are 68.2%, 10.2%, 20.5% and 1.1%, respectively, with the total FE for C_2H_4 and C_2H_6 of 78.4%. These FE of C_2H_4 and the total FE of C_2 are competitive with those reported for Cu–Cu^+ hybrids catalysts (Table S3†) with FE of C_2H_4 in the range from 10% to 59.3% and the FE of total C_2 in the range from 61% to 90.5% in recent works (Table S3†).[2,4,7,9,11,12,14,17,22,24,35] For example, Dinh *et al.* found that the FE of C_2H_4 and total C_{2+} were 70% and 83%, respectively, using

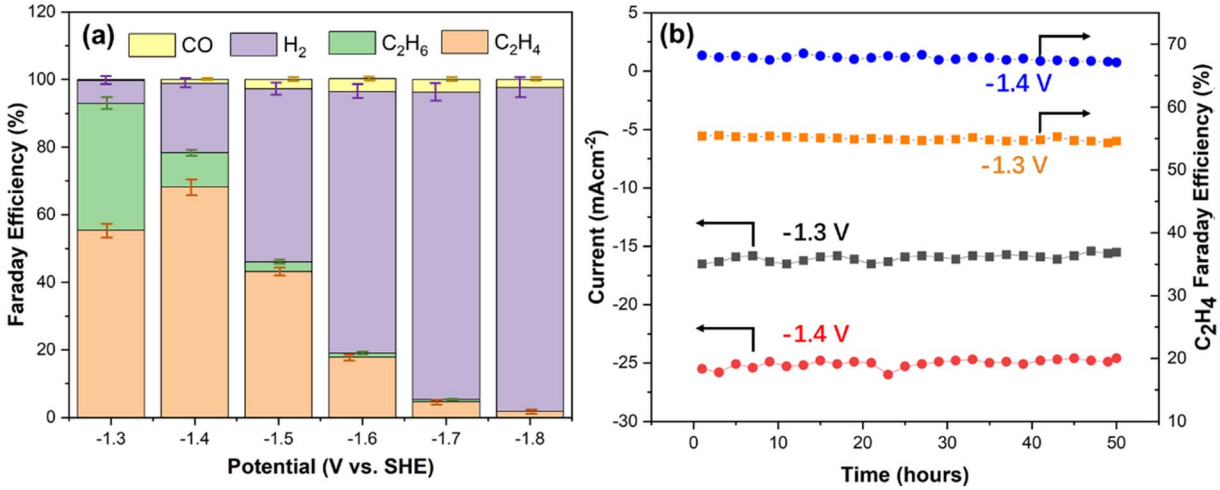

Fig. 5 (a) FE of the products generated by S10 at various potentials. (b) The FE of C_2H_4 and current density of the CO_2 ERR using the S10 catalyst at −1.3 V and −1.4 V *vs.* SHE, respectively.

the hydroxide-modified Cu nanocatalyst in 7 M KOH at −0.55 V *vs.* relative hydrogen electrode (RHE) by a flow cell electrolyzer.[2] Wang *et al.* achieved 53% FE of C_2H_4 and 74% of total C_2 using Cu–CuO_x/carbon black catalyst in 0.1 M $KHCO_3$ electrolyte at −1.3 V *vs.* RHE.[4] A similar FE of 46% for C_2H_4 was observed in the case of CuO–Cu_2O/carbon black in 0.1 M $KHCO_3$ using a flow cell.[7] The highest FE of 59.5% for C_2H_4 and 90.5% for total C_2 were reported by Cuenya's group using Cu_x@Cu_2O on carbon paper as the catalyst in an H cell filled with 0.1 M $KHCO_3$ solution at −1.2 V *vs.* RHE.[11] In our case, however, at a potential of −1.5 V *vs.* SHE, the FE of C_2H_4, C_2H_6, H_2 and CO was 43.2%, 2.9%, 51.2% and 3.7%, respectively. The FE for C_2 products dramatically declined to less than 10% when the potential was close to or less than −1.6 V *vs.* SHE. It is obvious that the more negative the potential, the more the formation of H_2.

Considering the current density and FE efficiency of C_2H_4 products, the time dependence of the FE and current density of S10 for CO_2 ERR were investigated to evaluate the stability at the potential of −1.3 V and −1.4 V, respectively. The results (Fig. 5b) indicate that during continuous operation for 50 hours, both the FE of C_2H_4 and current density of the CO_2 ERR at these two potentials show almost no change. In addition, the SEM image of the catalyst after operating for 50 hours at −1.3 V *vs.* SHE is shown in Fig. S13.† It shows the similar nanoparticular structures on the rGO surface as those in the original catalyst (Fig. 2c). This result demonstrates the good stability of the Cu–Cu_2O/rGO catalyst. It has been reported that fullerenes can stabilize the catalytic CO_2 ERR performance of the Cu–Cu_2O–C_{60} catalyst.[14–16] Furthermore, it has been found that carbon-based materials, such as carbon layer,[7] carbon black[13] and CNTs,[17] could stabilize the Cu^+ species of the CuO_x@C and Cu_2O/CNTs since the carbon layer or CNTs can increase the electronic conductivity of Cu^+ catalyst, which enables the electrons from the external circuit to transfer to the surface and facilitate the timely conversion of the reactant molecules, thus suppressing the reduction of Cu^+ species.[7,13,17] Similarly, in our case, the rGO layer will enhance the electronic conductivity of Cu_2O, transfer the electrons to the catalyst surface and facilitate CO_2 reduction, thus suppressing the reduction of Cu^+ species.

In situ ATR-SEIRS of the CO_2 ERR

In order to understand the CO_2 ERR process on the Cu–Cu_2O/rGO catalyst, S10 was investigated by an *in situ* ATR-SEIRS setup (see details in the Experimental section). After running for 100 s, the FTIR spectra were recorded at −1.3 V *vs.* SHE. The interval for the spectra was 2 min. The spectra shown in Fig. 6 were recorded in the wavenumber range from 1400 to 2200 cm^{-1}. The FTIR peak at about 2050 cm^{-1} is assigned to the adsorbed *CO.[5,7,9] The peak at about 1750 cm^{-1} is indexed to O–C=O intermediates.[11–17] Also, the peak at about 1525 cm^{-1} comes from the O=C–C=O species, the key intermediate for the formation of C_2H_4 or other C_2 products.[24–30] It is obvious

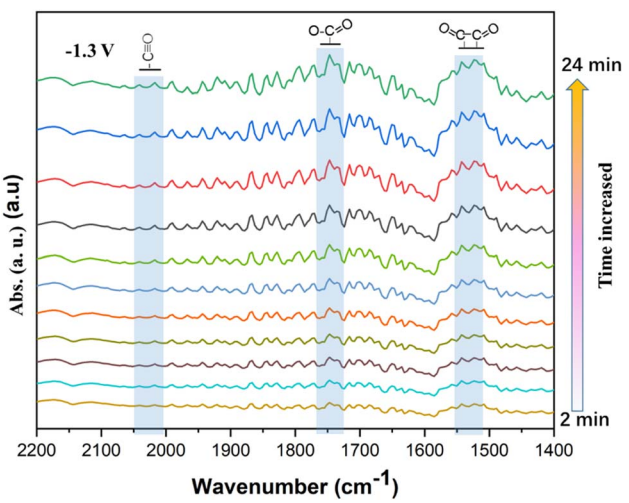

Fig. 6 Electrochemical *in situ* FTIR spectra of the S10 Cu–Cu_2O/rGO at a potential of −1.3 V *vs.* SHE. All the spectra were subtracted from the initial one (recorded after activation of 100 s).

that the O=C–C=O dimers are the dominant species on the surface. Previous works[11–17,24–30] indicate that the Cu^0/Cu^+ interfaces play a key role in the activation and CO dimerization, promoting the C_2 selectivity. Similarly, the conversion of CO_2 on Cu–Cu_2O/rGO by CO_2 ERR is achieved through the following steps: first, CO_2 is activated by Cu and Cu^+ to *CO and adsorbed on the catalyst surface. Two *CO species are coupled to form O=C–C=O and then further hydrated to C_2H_4 or C_2H_6. The rGO support enhances the electronic conductivity and protects the Cu^+ species. Therefore, the synergistic effect of Cu^0, Cu^+ and rGO of the Cu–Cu_2O/rGO catalyst contributes to its high selectivity and stability for the conversion of CO_2 to C_2H_4.

Conclusion

In summary, we prepared a Cu–Cu_2O/rGO catalyst from the CHNs/GO composite *via* an *in situ* electrochemical reduction process in a CO_2 ERR flow cell. The prepared Cu–Cu_2O/rGO demonstrated ~10 nm Cu–Cu_2O nanoparticles with Cu–Cu^+ combination anchored on the surface of rGO. These Cu–Cu^+ species are desirable for the activation of CO_2 and dimerization of C–C species, then selectively facilitating the formation of C_2H_4.[5,7,9–17,24–30] Due to these advantages, this Cu–Cu_2O/rGO catalyst presented highly selective CO_2 ERR to convert CO_2 to C_2H_4 in a flow-cell model. At −1.3 V *vs.* SHE, it shows an FE of 55.4% and 37.6% for C_2H_4 and C_2H_6, respectively, with a total C_2 FE of 93%. At −1.4 V *vs.* SHE, it shows an FE of 68.2% and 10.2% for C_2H_4 and C_2H_6, respectively, with a total C_2 FE of 78.4%. It also presents a good stability. This may provide a facile way to design Cu-based catalysts for selectively converting CO_2 to C_2H_4 *via* CO_2 ERR.

Data availability

The authors confirm that the data supporting the findings of this study are provided within the article and its ESI.† Raw data that support the findings of this study are available from the corresponding author, upon request.

Author contributions

Chenxiang Peng: primary investigation, methodology, formal analysis, and original draft writing and editing. Bing Yao: analysis, writing, reviewing and editing. Lei Wang: writing, reviewing and editing. Xinyi Wan: conceptualization, supervision, reviewing and editing, resources.

Conflicts of interest

There are no conflicts to declare.

Acknowledgements

This work was supported by the National Key Research and Development Program of China (2023YFB3810900).

References

1 C. P. O'Brien, R. K. Miao, A. S. Zeraati, G. Lee, E. H. Sargent and D. Sinton, *Chem. Rev.*, 2024, **124**, 3648.
2 C.-T. Dinh, T. Burdyny, M. G. Kibria, A. Seifitokaldani, C. M. Gabardo, F. P. de Arquer, A. Kiani, J. P. Edwards, P. D. Luna, O. S. Bushuyer, C. Zuo, R. Quintero-Bermudez, Y. Pang, D. Sinton and E. H. Sargent, *Science*, 2018, **360**, 783.
3 Y. Yang, Z. Tan and J. Zhang, *Chem.–Asian J.*, 2022, **17**, e202200893.
4 F. Yang, W. Fang, Q. Wang, P. Deng and B. Y. Xia, *ACS Sustainable Chem. Eng.*, 2022, **10**, 4677.
5 X. Chen, Y. Zhao, J. Han and Y. Bu, *ChemPlusChem*, 2023, **88**, e202200370.
6 E. Andreoli, *Nat. Catal.*, 2021, **4**, 8.
7 V. S. R. K. Tandava, M. C. Spadaro, J. Arbiol, S. Murcia-López and J. R. Morante, *ChemSusChem*, 2023, **16**, e202300344.
8 B. Yin, C. Wang, S. Xie, J. Gu, H. Sheng, D.-X. Wang, J. Yao and C. Zhang, *Angew. Chem., Int. Ed.*, 2024, **63**, e202405873.
9 D. Gao, I. Sinev, F. Scholten, R. M. Arán-Ais, N. J. Divins, K. Kvashina, J. Timoshenko and B. R. Cuenya, *Angew. Chem., Int. Ed.*, 2019, **58**, 17047.
10 R. Zhang, J. Zhang, S. Wang, Z. Tan, Y. Yang, Y. Song, M. Li, Y. Zhao, H. Wang, B. Han and R. Duan, *Angew. Chem., Int. Ed.*, 2024, **63**, e202405733.
11 H. Liu, C. Yang, T. Bian, H. Yu, Y. Zhou and Y. Zhang, *Angew. Chem., Int. Ed.*, 2024, **63**, e202404123.
12 X. Yuan, S. Chen, D. Cheng, L. Li, W. Zhu, D. Zhong, Z.-J. Zhao, J. Li, T. Wang and J. Gong, *Angew. Chem., Int. Ed.*, 2021, **60**, 15344.
13 Z. Wang, L. Xu, Y. Zhou, Y. Liang, J. Yang, D. Wu, S. Zhang, X. Han, X. Shi, J. Li, Y. Yuan, P. Deng and X. Tian, *Chem. Soc. Rev.*, 2024, **53**, 6295.
14 B. Zhao, F. Chen, C. Cheng, L. Li and B. Zhang, *Adv. Energy Mater.*, 2023, **13**, 2204346.
15 J. Zheng, L. Huang, C.-H. Cui, Z.-C. Chen, X.-F. Liu, X. Duan, X.-Y. Cao, T.-Z. Yang, H. Zhu, K. Shi, P. Du, S.-W. Ying, C.-F. Zhu, Y.-G. Yao, G.-C. Guo, Y. Yuan, S.-Y. Xie and L.-S. Zheng, *Science*, 2022, **376**, 288.
16 I. Shown, H.-C. Hsu, Y.-C. Chang, C.-H. Lin, P. K. Roy, A. Ganguly, C.-H. Wang, J.-K. Chang, C.-I. Wu, L.-C. Chen and K.-H. Chen, *Nano Lett.*, 2014, **14**, 6097.
17 X. Lv, Q. Liu, J. Wang, X. Wu, X. Li, Y. Wang, J. Yan, A. Wu and H. B. Wu, *Appl. Catal., B*, 2023, **324**, 122272.
18 Y. Luo, J. Huang, J. Jin, X. Peng, W. Schmitt and I. Ichinose, *Chem. Mater.*, 2006, **18**, 1795.
19 H. Huang, Z. Song, N. Wei, L. Shi, Y. Mao, Y. Ying, L. Sun, Z. Xu and X. Peng, *Nat. Commun.*, 2013, **4**, 3979.
20 W. Lu, W. Sun, X. Tan, L. Gao and G. Zheng, *Catal. Commun.*, 2019, **125**, 98.
21 Y. Deng, A. D. Handoko, Y. Du, S. Xi and B. S. Yeo, *ACS Catal.*, 2016, **6**, 2473.
22 L. Wang, Z. Chen, Y. Xiao, L. Huang, X. Wang, H. Fruehwald, D. Akhmetzyankov, M. Hanson, Z. Chen, N. Chen, B. Billinghurst, R. D. L. Smith, C. V. Singh, Z. Tan and Y. A. Wu, *Nat. Commun.*, 2024, **15**, 7477.

23 M. Sookhakian, M. A. Teridi, G. B. Tong, P. M. Woi, M. Khalil and Y. Alias, *ACS Appl. Nano Mater.*, 2021, **4**, 12737.
24 Y. Zhang, Y. Chen, X. Wang, Y. Feng, Z. Dai, M. Cheng and G. Zhang, *Nat. Commun.*, 2024, **15**, 5172.
25 Y. Kim, S. Park, S.-J. Shin, W. Choi, B. K. Min, H. Kim, W. Kim and Y. J. Hwang, *Energy Environ. Sci.*, 2020, **13**, 4301.
26 L. Zhang, Y. Men, B. Wu, Y. Feng, C. Song, S. Liu, J. Wang, W. An and T. T. Magkov, *Top. Catal.*, 2023, **66**, 1527.
27 W. Fang, R. Lu, F.-M. Li, C. He, D. Wu, K. Yue, Y. Mao, W. Guo, B. You, F. Song, T. Yao, Z. Wang and B. Y. Xia, *Angew. Chem., Int. Ed.*, 2024, **63**, e202319936.
28 F. S. Roberts, K. P. Kuhl and A. Nilsson, *Angew. Chem., Int. Ed.*, 2015, **54**, 5179.
29 M. Bisztyga-Szklaz, K. Mech, M. Mzrzec and R. Kalenarev, *Materials*, 2021, **14**, 3171.
30 Y. Zhao, X. Zu, R. Chen, X. Li, Y. Jiang, Z. Wang, S. Wang, Y. Wu, Y. Sun and Y. Xie, *J. Am. Chem. Soc.*, 2022, **144**, 10446.
31 A. Salverda, S. Abner, E. Mena-Morcillo, A. Zimmer, A. Elsayed and A. Chen, *J. Phys. Chem. C*, 2023, **127**, 7151.
32 R. Al-Gaashani, A. Najjar, Y. Zakaria, S. Mansour and M. A. Atieh, *Ceram. Int.*, 2019, **45**, 14439.
33 Q.-J. Wu, J. Liang, Y.-B. Huang and R. Cao, *Acc. Chem. Res.*, 2022, **55**, 2978.
34 H. S. Jeon, S. Kunze, F. Scholten and B. R. Cuenya, *ACS Catal.*, 2018, **8**, 531.
35 G.-Y. Duan, X.-Q. Li, G. R. Ding, L.-J. Han, B.-H. Xu and S.-J. Zhang, *Angew. Chem., Int. Ed.*, 2023, **61**, e202110657.
36 B. Beslsa, L. Xia, V. Golovanova, B. Polesso, A. Pinilla-Sánchez, L. S. Martin, J. Ye, C. T. Dinh and F. P. G. de Arquer, *Nat. Rev. Mater.*, 2024, **9**, 535.
37 Z. Chen, G. Zhang, H. Chen, J. Prakash, Y. Zheng and S. Sun, *Renewable Sustainable Energy Rev.*, 2022, **155**, 111922.